TECHNICAL ARTICLE

Design and Performance of a Laboratory Pneumatic Gun for Soil Ballistic Applications

A. Cave, S. Roslyakov, M. Iskander, and S. Bless

Civil & Urban Engineering, New York University Polytechnic School of Engineering, Brooklyn, NY

Keywords
Gas Gun, Projectile, Ballistics

Correspondence
M. Iskander
Civil & Urban Engineering
NYU Polytechnic School of Engineering
Brooklyn, NY 11201, USA
Email: iskander@poly.edu

Received: April 25, 2013;
accepted: March 12, 2014

doi:10.1007/s40799-016-0055-3

Abstract

A laboratory gun that uses compressed gas as its propellant was designed and tested for the study of small projectiles traveling in soils with initial velocities ranging from 50 to 200 m/s. The gun employed the use of air or helium with an electrically triggered, pneumatically piloted, solenoid valve. The triggering system was designed to provide remote activation. A photo gate speedometer was utilized to measure the exit velocity of each projectile. Details of the electro-pneumatic control system are presented in this paper along with the design of the gun assembly and its subsystems. The effects of different design parameters, including muzzle length, projectile mass, propellant type, and volume of compressed gas utilized, on projectile velocity were investigated. Statistical analysis of the gun performance is presented. The gun is currently being used to visualize the fundamental physics of rapid earth penetration in soils, using transparent soils.

Introduction

For years, travel of projectiles in soils has intrigued engineers and scientists. The interest in the subject initially stemmed from military applications. Over the past century, research has also been motivated by other applications which include: subsurface investigation of soil and rock, particularly at inaccessible locations, installation of deep sea anchors and foundations, nuclear waste disposal, mining, and aircraft landing studies. Several important studies of projectile penetration in different materials have been published, including penetration into metals,[1] rocks,[2] and soils.[3]

A research initiative has been undertaken at New York University Polytechnic School of Engineering to employ transparent soils in the study of fundamentals of soil–projectile interaction during rapid penetration into sand. Transparent soils made of fused quartz saturated with a matched refractive index fluid were employed.[4,5] Deformation fields are obtained by illuminating a plane within the soil using a coherent laser light source, which produces a unique speckle pattern.[6,7,8] Digital image correlations of successive speckle images are employed to obtain the displacement field.[7,9,10]

The objective of this study was to build and test a laboratory gun that was capable of propelling small-diameter projectiles with speeds of 50–200 m/s into a predetermined plane of interest in the transparent soil target, in a controlled and repeatable manner (Fig. 1). The laboratory in which gun experiments were conducted was located next to a classroom; therefore, operation must be below ear protection requirements and nonhazardous. The initial velocity prior to impact had to be measured, for each shot.

This paper presents the procedures taken to design a laboratory gas gun, along with its performance. It is hoped that the methodology would be useful to a variety of users as gas guns are employed in different research applications, but their simplified design procedures are rarely available.

Selection of Gun Type

Several mechanisms for propulsion of the projectile were investigated. Simplicity of design, accuracy of trajectory, and repeatability of velocity were the

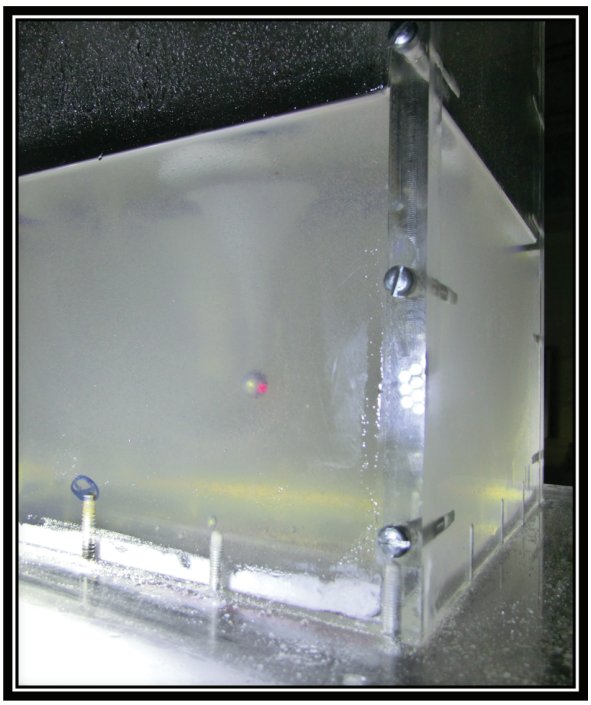

Figure 1 Post-test image of projectile embedded in transparent soil along with cavity formation.

main desired characteristics. Two types of guns were initially investigated: a gas gun[11,12] and an electromagnetic coil gun.[13] Both types met the sound level requirements. However, the gas gun was chosen because it did not require a high current and high voltage power supply. Laboratory grade compressed air and helium were available and relatively inexpensive from commercial gas suppliers. An added advantage is that gas guns could easily be triggered remotely.

Guns that use compressed gas as a propellant can be divided into two subtypes: the spring and piston and the reservoir type.[14] The spring and piston type is operated by rapidly compressing the gas behind a projectile during firing. Spring and piston pneumatic guns do not require a separate source of compressed gas as firing the gun compresses the gas and fires in the same action. This allows the gun to be lightweight and does not require connection to a pre-loaded gas cylinder. Reservoir-type pneumatic guns use the force from pre-compressed gas, stored in a reservoir chamber. At the time of triggering, a valve is opened releasing compressed gas from the pressurized reservoir. Speed of the projectile may be adjusted by varying the initial pressure and volume of the reservoir. The reservoir-type gas gun typically has a simpler design with less moving parts than the equivalent spring and piston gun. However the reservoir gun occupies more space as it requires a source of compressed gas. The reservoir type was selected because it offers the ability to adjust velocity without tinkering with mechanical components. The size of the gun was not a constraint because the gun was to be fixed in place within a laboratory environment.

A number of reservoir-type gas guns have been developed for propelling projectiles into sand. Borg et al.[15] employed an electro-pneumatic air gun with a barrel length of approximately 1.5 m that propelled small projectiles horizontally into dry sand (Borg, personal communication). Velocities of up to 150 m/s were achieved by employing a 500 cc chamber pressurized to 2.41 MPa (350 psi), which corresponded to an efficiency of approximately 50%. Thompson[11] also presented a mechanically triggered compressed gas gun that propelled a 2.8-kg cylindrical projectile with a conical nose at speeds of up to 150 m/s, vertically downward into a bed of sand. It employed a 3.25-m muzzle and a 4000-cc nitrogen gas chamber. A long projectile (penetrometer) was held in place prior to firing by O-ring seals above and below the pressurized chamber. The gun was fired by lowering the projectile until it exposed its top to the pressurized nitrogen gas within the chamber, which accelerated the projectile downward. Thompson's gun employed two notable features. First, the projectile itself comprised the firing valve. Second, the projectile housed an accelerometer that was employed to resolve the time-displacement curve. The gun presented in this paper fires vertically downwards similar to Thompson,[11] but employs a firing mechanism similar to that of Borg et al.[15]

Estimate of Muzzle Velocity for Reservoir-Type Gas Guns

A first estimate of the projectile velocity for a given barrel and chamber size can be made by neglecting losses and assuming that the sum of the projectile's potential energy and energy from isentropic expansion of the compressed gas through the gun barrel is equal to the projectile's kinetic energy, as follows:

$$\frac{mv^2}{2} = W_{\text{gas}} + mgl_{\text{b}} \tag{1}$$

where m is the mass of the projectile, v is the projectile exit velocity, g is acceleration due to gravity and l_{b} is barrel length. The work performed by expansion of a gas, W_{gas} as a function of its pressure and volume at

any point of time during the expansion is:

$$W_{\text{gas}} = \int pdV \tag{2}$$

where p is the instantaneous pressure and dV is the instantaneous volume. In an isentropic process pressure is related to volume according to Boyles' law, as follows:

$$pV^{\gamma} = \text{constant} \tag{3}$$

where V is the volume of the compressed air, and γ is the ratio of specific heats of heat capacity at constant pressure to heat capacity at constant volume, which is typically 1.4 for dry air and 1.66 for helium.[16] The pressure at any point in the expansion can be written as a function of volume using the initial pressure and initial volume p_o and V_o as follows:

$$p = p_o \left(\frac{V_o}{V}\right)^{\gamma} \tag{4}$$

Upon substituting Eq. 4 into Eq. 2 and evaluating the integral with the limits set to initial volume V_o and final volume $V_f = A\, l_b + V_o$, where A is the cross-sectional area of the muzzle, and l_b is the barrel length, the work done by expansion of the gas is obtained as:

$$W_{\text{gas}} = \frac{p_o V_o}{\gamma - 1}\left[1 - \left(\frac{V_o}{V_o + A l_b}\right)^{\gamma - 1}\right] \tag{5}$$

The muzzle velocity can thus be estimated by substituting the expression from Eq. 5 into Eq. 1 as follows:

$$v = \eta \sqrt{\frac{2}{m}\frac{p_o V_o}{(\gamma - 1)}\left[1 - \left(\frac{v_o}{v_o + A l_b}\right)^{(\gamma - 1)}\right] + 2 g l_b} \tag{6}$$

where, the efficiency term, η, is introduced to correct for all the neglected losses. An efficiency value of $\eta = 0.5$ was employed based on similar parameters from previous studies,[15] and later confirmed by actual results.

Gun Design

The design methodology used in this paper is simplified and limited to lower velocity regimes after which different effects cause deviation from calculated expectations. Other design procedures[17–19] have been published before and provide alternative procedures for single stage gas design. The gun consisted of (1) a frame to support it, (2) a pressure chamber, (3) an electro-pneumatic valve, and (4) a barrel, as follows.

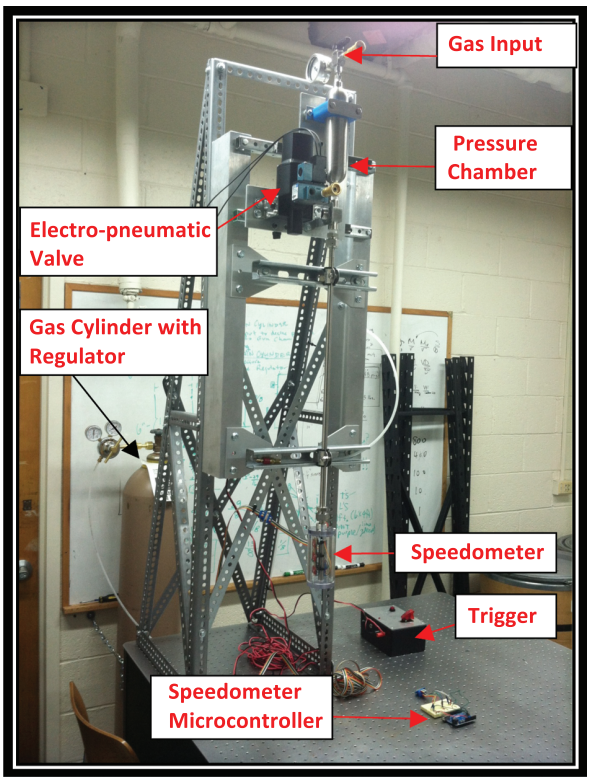

Figure 2 View of the electro-pneumatic gas gun.

The frame

The frame served to hold the gun over a transparent soil model, approximately 300-mm cube (Fig. 1), designed to rest on a rigidly mounted optical table (Fig. 2). Initially, consideration was given to separating the gun from the optical table in order to eliminate transfer of vibration from the gun to the model, by fastening the frame to either the floor or the ceiling. However, upon recognizing that the mass of the table was over 4 orders of magnitude larger than the projectile and that the selected reservoir-type method of operation produced negligible vibration, the frame was bolted to the optical table because it was the easiest and most efficient use of space.

The gun frame was a triangular truss structure built from 25 × 25 mm perforated galvanized steel angles. The frame was 1.5 m tall, with a 0.40 × 0.45 m base and was bolted to the optical table with eight 25 mm long ¼-20 inch bolts. A 200-mm offset was required between the plane of the barrel and the front of the frame, so that projectiles impact the model at its center. Thus, the gun apparatus was mounted on two 20 mm × 40 mm deep aluminum channels connected to the top portion of the frame.

Pressure chamber

The gas chamber-stored compressed gas used to propel the projectile through the barrel, mounted vertically above the gun. The effect of chamber size was investigated by employing two chambers, 300 and 500 cc. The chambers were rated 12.41 Mpa (1800 psi) and were made of stainless steel with 1/4-inch size female NPT connections on both sides. A two-way hand operated ball valve was connected at the top, such that the common port is connected to the chamber and the other two ports connect to the supply compressed gas regulator and a pressure gauge. The lower connection of the pressure chamber was connected to the electro-pneumatic valve. The chamber was supplied through a commercial compressed gas cylinder (air or helium). The chamber pressure was controlled using a pressure regulator attached to the cylinder.

The number of shots per cylinder can be approximated using ideal gas law as follows:

$$\left(\frac{n_2}{n_1}\right) = \left(\frac{P_2 V_2}{P_1 V_1}\right) \tag{7}$$

where n_2/n_1 is shots per compressed gas cylinder, V_1 is the volume of chamber, V_2 is the volume of the cylinder (49.9 L), P_1 is the chamber pressure, and P_2 is the supplied pressure of the cylinder (20 Mpa, 2900 psi). For the selected 300 cc chamber volume, and pressure of 1.03 Mpa (150 psi), the estimated number of shots per cylinder was approximately 3000.

Electro-pneumatic valve

An air-piloted single acting electro-pneumatically actuated normally closed ball valve was installed between the air reservoir and the barrel. The valve was actuated by a 12VDC solenoid and supplied with 1.03 Mpa (150 psi) pilot air from the compressed gas cylinder. When the valve is open, it releases the compressed gas to propel the projectile through the barrel.

The capacity coefficient, C_v (also known as valve flow coefficient), is a dimensionless index that is used by industrial designers to simplify the problem of control valve sizing.[20] For high-pressure differential gas flow where the downstream absolute pressure is less than half of the upstream pressure, C_v is expressed by:

$$C_v = \frac{Q}{13.9 \times C_f \times P_1 \sqrt{\frac{1}{(SG)T}}} \tag{8}$$

where P_1 is the upstream pressure (in reservoir). The critical flow factor, C_f that corresponds to geometric properties of the valve, was obtained as 0.98 from the manufacturer. The required capacity coefficient was calculated for the pressure range of interest by determining the flow rate (Q) needed for the expansion of gas into the barrel using the isentropic flow equations. In our experimental conditions, P_1 ranges from 0.14 to 1.72 MPa (20–250 psi), specific gravity (SG) was 1 and 0.138 for air and helium respectively, and the room temperature T was estimated as 532R (22°C). The flow rate, Q, was found in the range from 13.2 to 350 SCFM (standard cubic feet per minute) using Eq. 9. In SI units, the valve flow coefficient is known as K_v ($0.85C_v$) and A_v ($2.4 \times 10^{-5} C_v$), in mixed and coherent units respectively.[21] The required flow (Q) was found as follows:

$$Q = \frac{\left(\pi \frac{d^2}{4}\right) L_b}{t} \times \frac{P_{chamber} + P_{atm}}{P_{atm}} \tag{9}$$

where t is the time of travel in minutes within a barrel of diameter d, found by numerically integrating the distance computed using Eq. 6. This flow rate was converted to SCFM (at 21°C and atmospheric pressure) in order to find the C_v value (Eq. 8). The valve flow coefficient corresponding to the highest air demand (air as propellant, barrel length of 0.75 m and 500-cc chamber pressurized at 1.72 MPa (250 psi) was found to be 2.26. Therefore a *Swagelok SS-44 F6-33C* valve with a C_v of 2.6 was selected.

Barrel and projectile

A spherical projectile, 9.9 mm (0.390 inch) in diameter was selected for initial testing since the symmetry of that shape eliminates pitch and yaw concerns, resulting in a straighter trajectory in the target medium. Three different projectile materials were tested: aluminum, 440 stainless steel, and tungsten carbide, having nominal masses of 1, 4, and 8 g, respectively.

A smooth bore stainless steel tube having an outer diameter of 12.7 mm (0.50 inch) and an inner diameter of 10.16 mm (0.40 inch) was employed, which permitted 0.13 mm (0.005 inch) of clearance. The clearance and welding of this barrel were believed to have contributions to efficiency loss.

The effect of barrel length was investigated by employing three barrels, 0.3, 0.6, and 0.75 m long. The barrel was loaded at its top, where it was connected to the pneumatic valve. This connection had to be repeatedly disconnected and reconnected by hand, to insert the projectile prior to each shot. Thus, a flange was welded to the top of the barrel and a

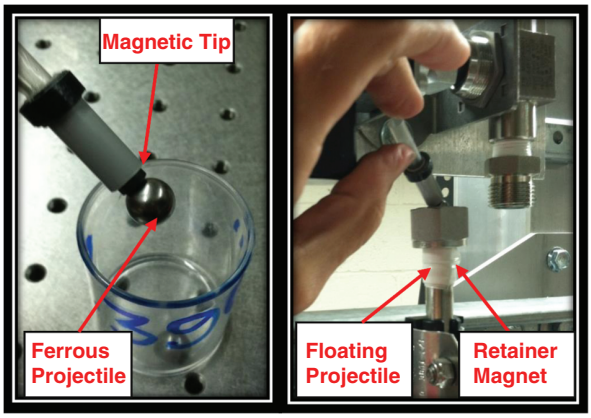

Figure 3 Magnetic loading tool (left) and loading of the projectile into the connection (right).

female collar was fitted under the flange and threaded to the male fitting connected to the pneumatic trigger (Fig. 3). A positive seal is accomplished by the compression of a rubber O-ring (70 durometer) affixed to the male side of the connection.

In order to load the barrel, the connection was separated, lowered, and misaligned to insert the projectile (Fig. 3). The projectile was held in place until firing by one of two mechanisms. For nonferrous materials a square-ring (an O-ring with a square cross section) having an ID of 8.5 mm and an OD of 12 mm was stretched over the projectile to hold it in place over the flange. For ferrous materials a magnetic retainer was taped to the outside of the barrel. The magnetic force was sufficient to prevent free-fall of a projectile, but only if it was loaded slowly. Thus, a loading tool made of two concentric cylinders with the inner one having a magnet at its tip which held the ferrous projectile. The outer cylinder was used to carefully separate the inner tube from the projectile after it was positioned by pushing the projectile into the barrel where the retainer magnet attracted it and suspended it within the barrel (Fig. 3)

Trigger Design

A +12VDC, 500-mA electrical signal was required to energize the solenoid valve. The required signal was sent via a *Parallax Basic Stamp* microcontroller that was powered using a 9VDC battery; it monitored a series of input pins continuously and energized the solenoid when several conditions were met (Fig. 4). First, a safety switch had to be toggled on which set pin-2 status to high. Second, after a 5 s delay; a bi-color LED on pin 1–0 was switched from red to green. Finally, an ignition switch must be pressed in order to set pin-3 to high. When all conditions are met pin 10 sends a 5-V signal to a *2 N4401* switching transistor that delivers the required signal to the solenoid valve. The trigger electronics were installed inside of a plastic enclosure with the interface switches mounted on a top panel.

Speedometer Design

The gun required some means of measuring the projectile speed as it leaves the barrel. The speedometer consisted of three infrared *photo-sensor* pairs mounted on a 0.15 m long and 0.5 inch diameter extension section that was threaded in line with the gun barrel at its end. The speedometer and its electronics were contained in a cylindrical enclosure mounted at the exit of the gun barrel (Fig. 5).

The photo-sensors were mounted in front of holes drilled in the barrel extension cylinder. One side of each photo-sensor contained infrared emitters while the other contained phototransistor receivers. The three pairs of photo-sensors were fixed 30 mm apart. As long as the infrared light beam passed uninterrupted from the emitter to the phototransistor, the signal remained high. When the projectile blocks the beam of light, the signal goes low. A microcontroller was used to receive and process the digital signals of the photo-sensors and to display the velocity data to the computer via USB. The average speed of a projectile passing through the tube was measured by dividing the distance between two pairs of photo-sensors by the amount of time in between each sensor's status change (Fig. 6). This resulted in three reported speeds, which provided an additional measure of redundancy and also allowed the user to compute average acceleration between the first and second pair of sensors.

The speedometer employed an *Arduino Uno* microcontroller, which had a clock resolution of 4 microseconds. This was also the time required to check the state of the sensor pins and the time required to make a time stamp. The actual gate separation distance was directly measured by an LVDT used as a caliper by observing the status changes of the sensors while manually pushing of a projectile through the barrel. This empirical determination of activation points allowed for elimination of uncertainty due to infrared beam width. The uncertainty in the distance, D_u, due to the micro-controllers sampling rate and the LVDT resolution, in percent, can be expressed as:

$$D_u = \frac{\pm (V)\,(t_{cl}) \pm U_{lvdt}}{d} \times 100 \qquad (10)$$

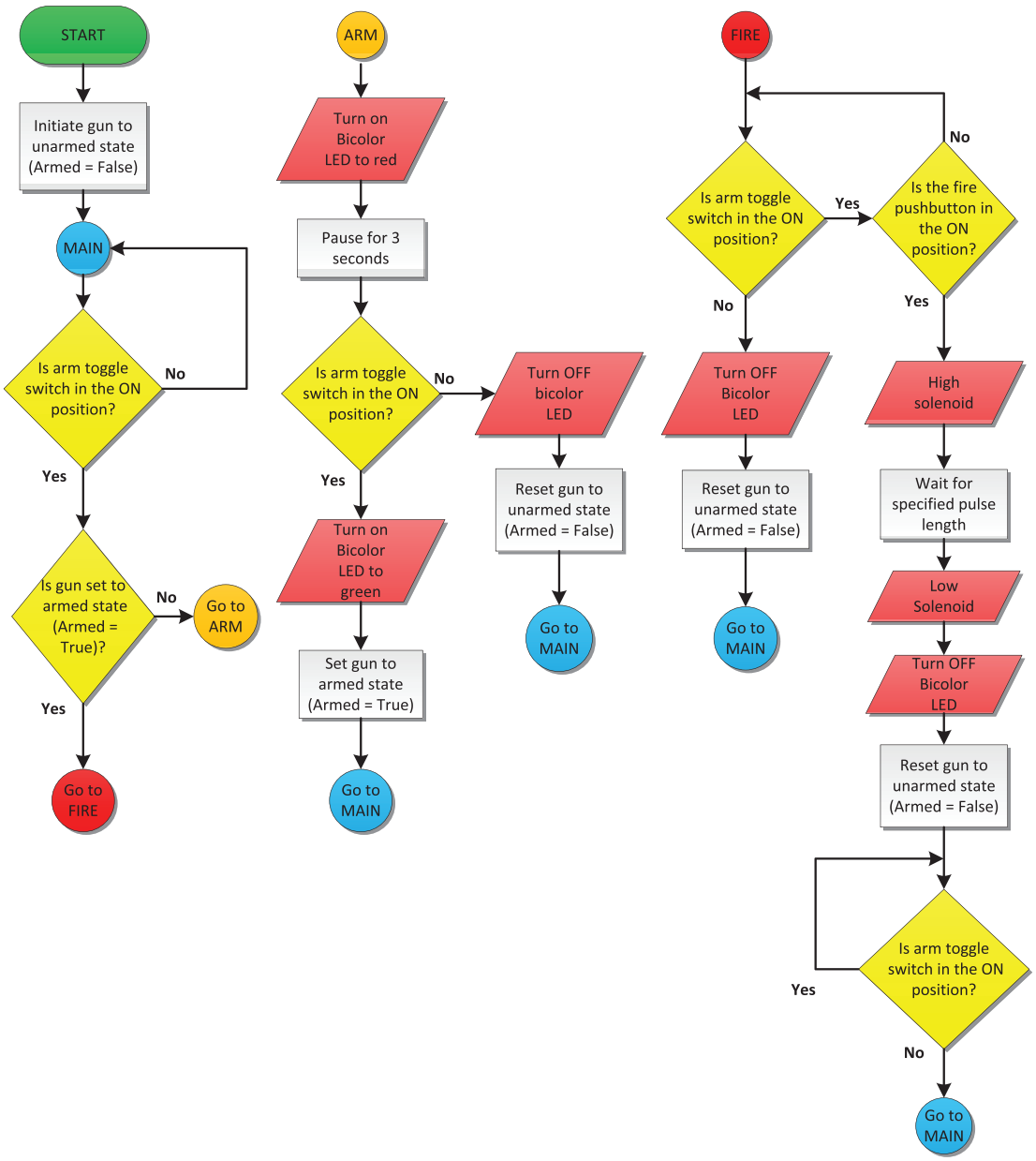

Figure 4 Flow chart for trigger operation.

where t_{cl} is the clock resolution of the microcontroller (4×10^{-6} s) , V is the velocity of the projectile, U_{lvdt} is the resolution of the LVDT taken as 10^{-5} m, and d is the actual gate separation distance (0.03). The uncertainty in time, T_u, in percent, can be expressed as follows:

$$T_u = \frac{t_{cl}}{d/v} \times 100 \tag{11}$$

The total uncertainty is the sum of both time and distance uncertainties. However, the probable uncertainty may be found by employing Taylor's theorem as follows:

$$U = \sqrt{T_u^2 + D_u^2} \tag{12}$$

For speeds of 50, 100, and 200 m/s the probable uncertainty is approximately 0.96% (±0.5 m/s), 1.9% (±1.9 m/s), and 3.8% (±7.6 m/s), respectively.

Testing Method and Results

The gun was put through a number of tests to obtain muzzle velocity as a function of chamber

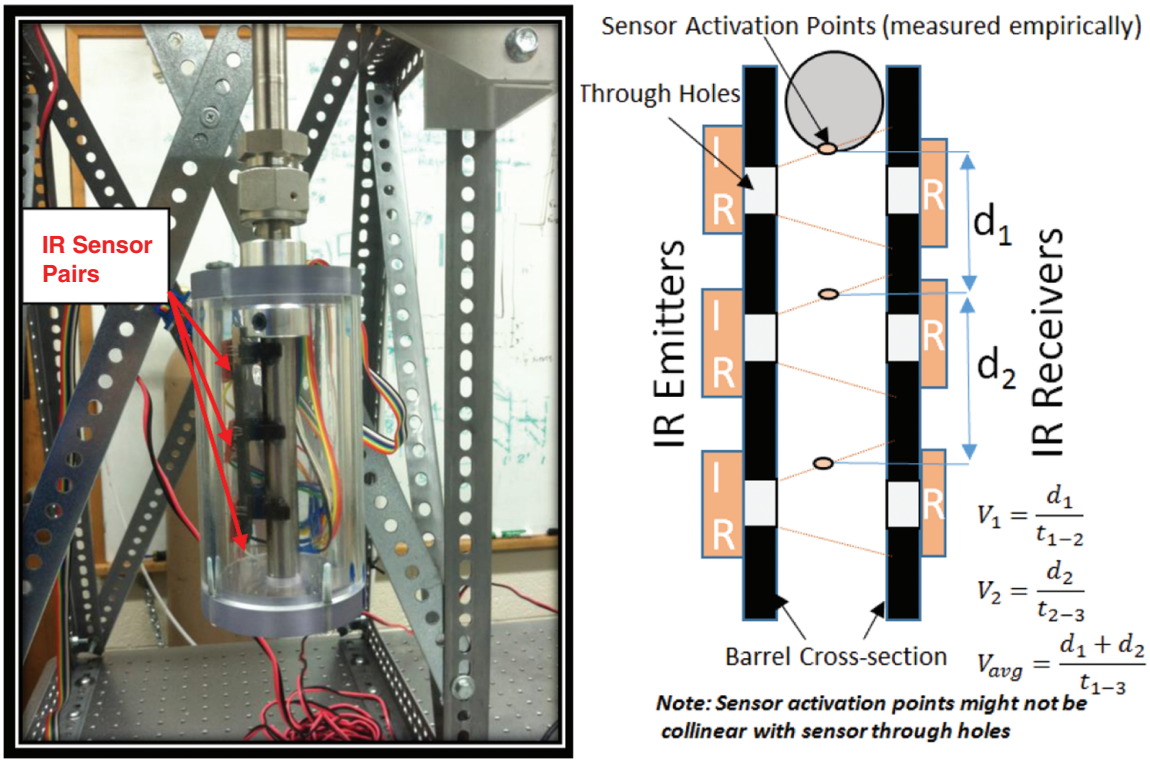

Figure 5 Final assembly of the speedometer at the end of the barrel.

pressure for several different configurations using two gases. The air-propellant tests consisted of eight shots for varying pressures from 0 to 0.965 MPa (0–140 psi) while changing of the barrel length, projectile type, and chamber volume. The helium-propellant test configuration consisted of five shots of varying pressure from 0 to 1.72 MPa (0–250 psi) while changing the projectile type and barrel length. The effects of chamber volume were not tested with helium because of the small velocity differences from the air-based tests.

Measured velocity with air propellant

Initially, predictions for gun performance were made using Eq. 6 for ideal gas expansion (Fig. 7). The actual effect of chamber volume was investigated using two chambers of 300 and 500 cc by performing eight shots at each test pressure with a constant projectile mass of 4 g and barrel length of 0.76 m (Fig. 8). At pressure bellow 0.7 MPA (100 psi) a smaller chamber yields higher velocity; however, the effects of chamber size were small, therefore all subsequent tests employed a 300-cc chamber. The observed velocities are below the theoretical values owing to efficiency losses.

Three barrel lengths were also tested by performing eight shots at each varying pressure with constant projectile mass of 4 g and a chamber volume of 300 cc (Fig. 9). The barrel lengths affected the velocity of the projectile as predicted by ideal expansion, in which the longest barrel should provide the largest velocity as a result of longer applied acceleration in the barrel.

Three projectile masses were also tested by performing eight shots at each varying pressure with a constant barrel length of 0.76 m and chamber volume of 300 cc (Fig. 10). As expected, lighter projectiles travel faster as predicted by the conservation of energy law.

Measured velocity with helium propellant

Three barrel lengths were tested at varying pressures with constant projectile mass of 4 g and chamber volume of 300 cc (Fig. 11). The three projectile masses were tested by performing five shots at each varying pressures with a constant barrel length of 0.76 m and chamber volume of 300 cc (Fig. 12). Again lighter projectiles, and longer muzzles, contribute to higher velocities but the rate of increase is different for air and helium.

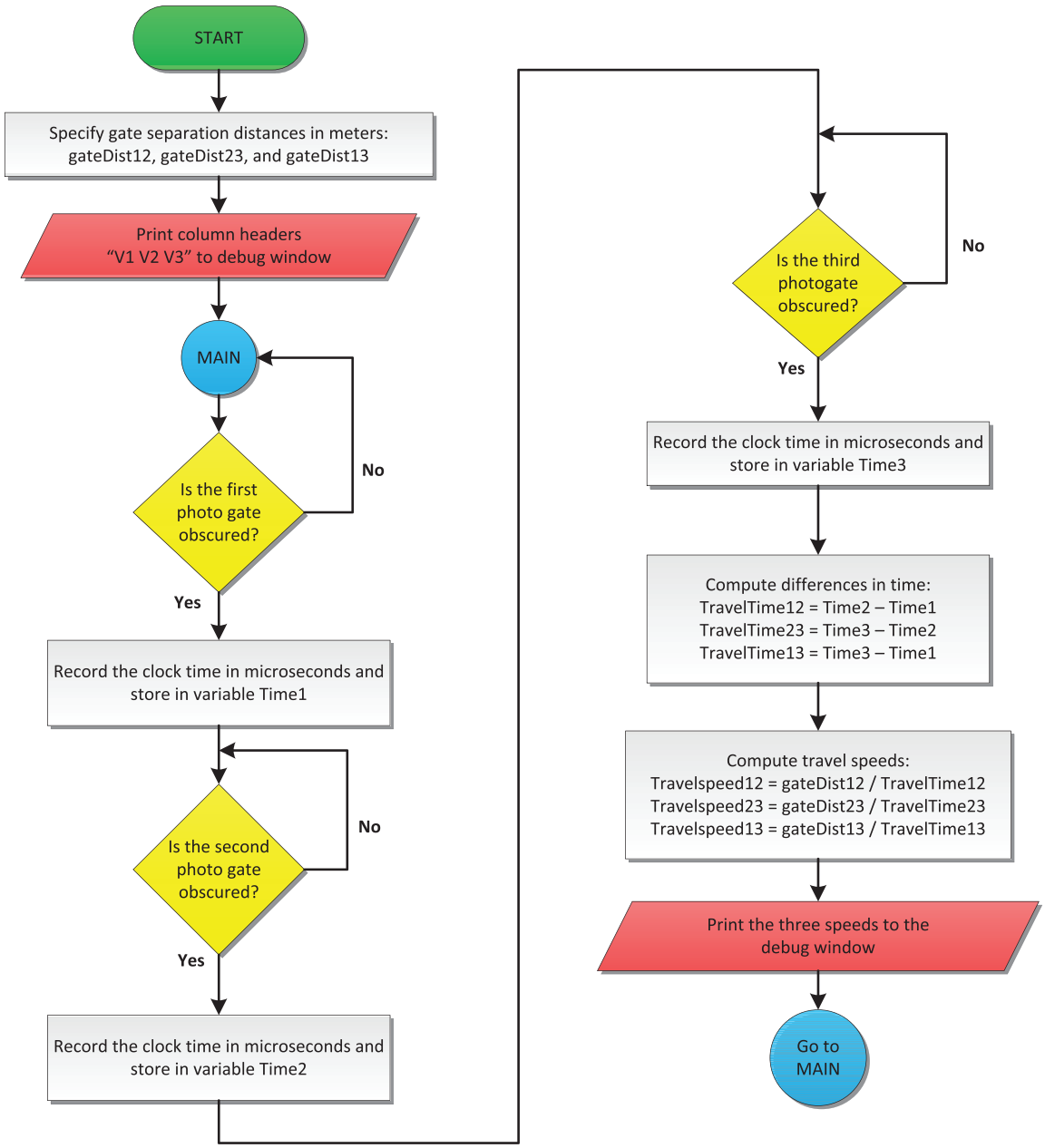

Figure 6 Flow chart for speedometer operation.

Efficiency

The measured velocities compared with the theoretical velocities (Fig. 7) are computed using ideal expansion (Eq. 6,when $\eta = 1$), and the results are expressed in terms of percent efficiency in Tables 1 and 2 for air and helium gases, respectively. The measured efficiencies averaged 57 and 70% for air and helium, respectively, with barrel length and chamber volume having a small effect on efficiency. However, the efficiency increased as the projectile mass increased and it decreased somewhat as pressure increased. Energy loss could have possibly resulted from choked flow at the valve (which has a finite opening time) or blow by of gas around the projectile in the muzzle. Additionally, the welding of the flanges to the muzzle causes a small misalignment on the order of 1°, which at high velocities may cause loss of efficiency due to collision of the projectile with this weld imperfection.

Results for helium gas exhibited similar trend to air but with helium exhibiting 15% better efficiency

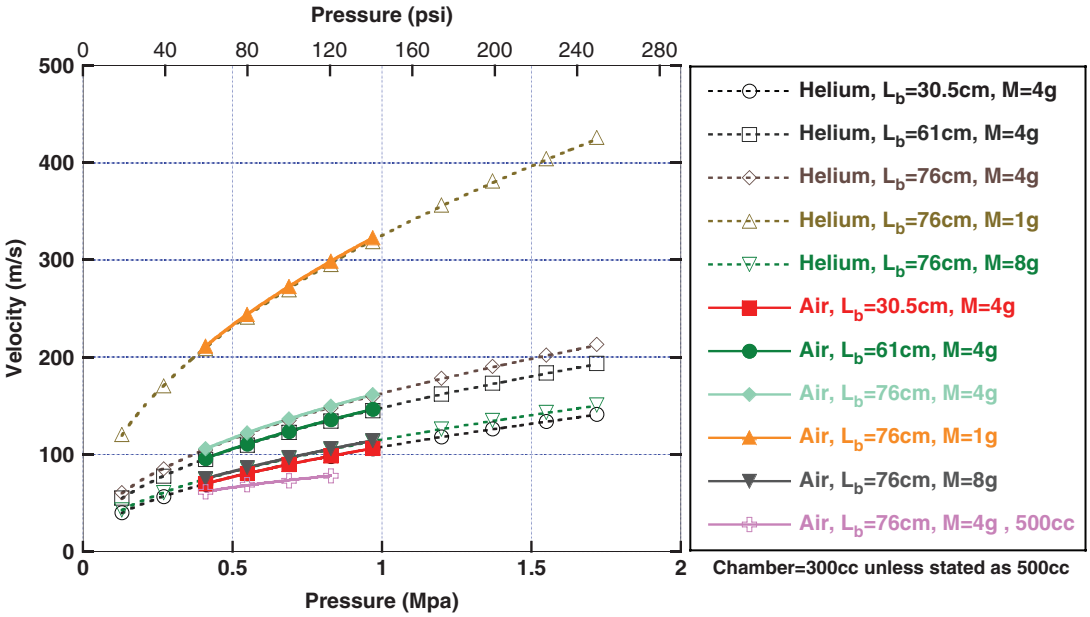

Figure 7 Theoretical velocities based on work done by ideal gas expansion.

Table 1 Energy efficiency for air tests

	Experimental velocity/theoretical velocity, %							
	$M = 4$ g, Chamber = 300 cc			$M = 4$ g, $L_b = 76$ cm	Chamber = 300 cc, $L_b = 76$ cm			
Pressure (Mpa)	$L_b = 30.5$ cm	$L_b = 61$ cm	$L_b = 76$ cm	Chamber = 500 cc	$M = 1$ g	$M = 4$ g	$M = 8$ g	Average
0.41	56.08	60.51	62.74	56.59	54.81	62.74	82.25	62.25
0.55	57.85	54.81	56.06	55.03	53.25	56.06	81.93	59.28
0.69	51.79	51.68	53.83	51.90	51.51	53.83	84.43	57.00
0.83	49.45	49.96	51.35	50.86	50.77	51.35	79.88	54.80
0.97	49.28	46.87	49.94	N/A	50.07	49.94	77.54	53.94
Average	52.89	52.77	54.78	53.56	52.08	54.78	81.21	57.45

than air. The efficiency is greater for helium than for air and is higher for low velocity than for high velocity, which implies that the deviation from ideal gas behavior is caused by propagation effects. The flow rate through the valve is greater for helium than for air because helium has a much higher sound speed than air (920 versus 340 m/s). The adiabatic model (Eq. 6) does not consider propagation effects owing to sound speed limitations from the two gases. Nevertheless, it can still be used to estimate the theoretical velocity of helium propellant shots, because these effects become more relevant after velocity exceeds one third of sound speed, which with helium is well below intended experimental velocities. Failure to include propagation effects results in reduced efficiency, particularly for air and as the pressure increases (Tables 1 and 2). In principal, for higher velocities, as pressure increases, use of a one-dimensional (1D) adiabatic propagation law may provide better velocity estimations, and in return a better estimate of true efficiency.

Repeatability

The relative standard deviation defined as the standard deviation normalized by the average velocity and expressed as a percent is presented in Tables 3 and 4. The relative standard deviation ranged between 1.57 and 7.70% for tests with air and 0.36 and 21.34% for tests with helium, with an average of 3.72 and 3.89, respectively. Some of the discrepancy in repeatability may be caused by the uncertainty in the speedometer measurements discussed previously, and the use of a manually operated pressure gage.

Table 2 Energy efficiency for helium tests

	Experimental velocity/theoretical velocity, %						
	$M = 4$ g, Chamber = 300 cc			Chamber = 300 cc, $L_b = 76$ cm			
Pressure (Mpa)	$L_b = 30.5$ cm	$L_b = 61$ cm	$L_b = 76$ cm	$M = 1$ g	$M = 4$ g	$M = 8$ g	Average
0.13	95.99	79.61	72.11	65.19	72.11	67.65	75.44
0.27	77.20	73.06	76.05	61.65	76.05	80.11	74.02
0.41	77.85	80.21	74.04	55.47	74.04	83.23	74.14
0.55	73.24	78.18	79.58	53.89	79.58	82.91	74.56
0.69	67.99	75.48	78.39	52.13	78.39	85.44	72.97
0.83	67.94	72.06	78.65	51.38	78.65	80.84	71.59
0.97	69.38	72.46	72.94	50.68	72.94	78.47	69.48
1.20	65.43	70.71	74.44	48.44	74.44	81.98	69.24
1.37	64.63	68.71	72.38	47.32	72.38	79.24	67.44
1.55	64.04	67.69	69.34	46.40	69.34	82.34	66.53
1.72	63.32	66.64	70.82	46.16	70.82	79.87	66.27
Average	66.27	66.86	66.92	65.62	75.35	79.87	70.15

Table 3 Relative standard deviation of exit velocities for air tests

	Standard deviation/average speed, %							
	$M = 4$ g, Chamber = 300 cc			$M = 4$ g, $L_b = 76$ cm	Chamber = 300 cc, $L_b = 76$ cm			
Pressure (Mpa)	$L_b = 30.5$ cm	$L_b = 61$ cm	$L_b = 76$ cm	Chamber = 500 cc	$M = 1$ g	$M = 4$ g	$M = 8$ g	Average
0.41	6.39	4.40	4.66	4.17	3.93	4.66	5.21	4.77
0.55	6.22	4.07	2.15	3.83	2.80	2.15	2.37	3.37
0.69	6.22	2.71	1.59	2.22	3.81	1.59	1.66	2.83
0.83	7.37	4.70	2.28	3.42	2.65	2.28	1.57	3.47
0.97	7.70	5.47	3.39	N/A	1.71	3.39	3.33	4.17
Average	5.53	4.27	2.81	3.41	2.98	2.81	2.83	3.72

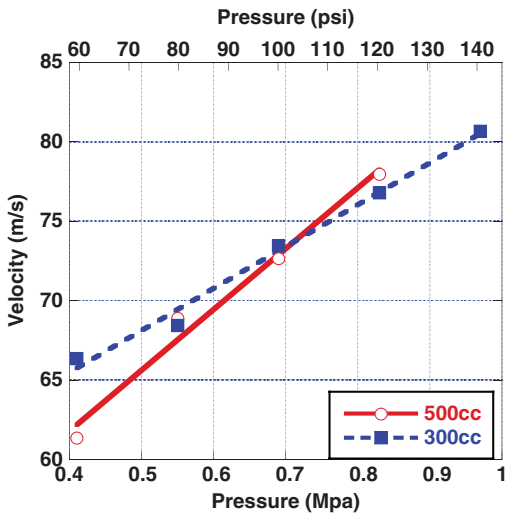

Figure 8 Effects of chamber size on projectile with air propellant ($L_b = 76$ cm, $M = 4$ g).

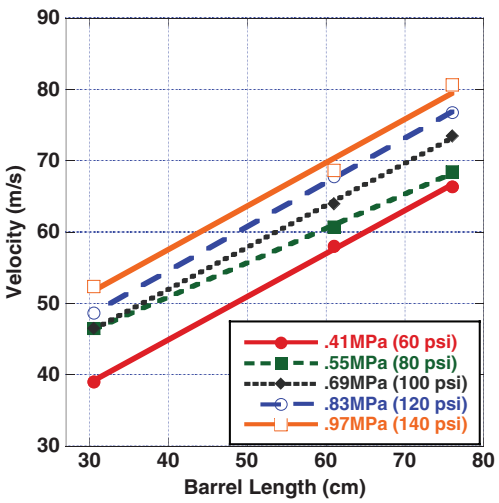

Figure 9 Effect of different barrel length on velocity with air propellant ($V = 300$ cc, $M = 4$ g).

The relative standard deviations for different configurations were combined into two data sets, representing tests with air and helium. Statistical analysis software[22] was employed to determine the ideal probability density distribution of each data set. The normal Gaussian distribution ranked 9 and 12

Table 4 Relative standard deviation of exit velocities for helium tests

	Standard deviation/average speed, %						
	$M = 4$ g, Chamber = 300 cc			Chamber = 300 cc, $L_b = 76$ cm			
Pressure (Mpa)	$L_b = 30.5$ cm	$L_b = 61$ cm	$L_b = 76$ cm	$M = 1$ g	$M = 4$ g	$M = 8$ g	Average
0.13	0.94	0.53	11.53	5.90	11.53	21.34	8.63
0.27	1.47	2.25	5.02	6.50	5.02	13.64	5.65
0.41	0.54	2.22	5.80	6.16	5.80	2.54	3.84
0.55	0.65	1.92	5.26	4.53	5.26	4.51	3.69
0.69	0.80	1.48	6.30	1.69	6.30	4.09	3.44
0.83	0.43	1.01	3.83	2.65	3.83	3.62	2.56
0.97	1.38	1.28	8.24	3.53	8.24	0.98	3.94
1.20	0.36	0.84	4.92	2.10	4.92	1.85	2.50
1.37	1.72	1.02	2.55	3.60	2.55	6.40	2.97
1.55	1.87	1.09	4.24	3.31	4.24	1.58	2.72
1.72	0.75	0.57	2.95	5.11	2.95	4.82	2.86
Average	0.99	1.29	5.51	4.10	5.51	5.94	3.89

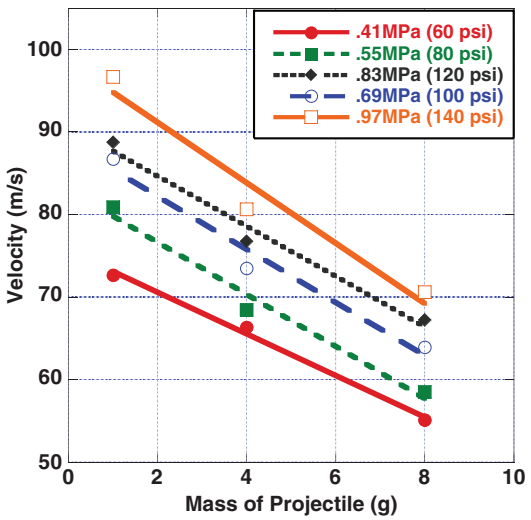

Figure 10 Effect of different projectile mass on velocity with air propellant ($L_b = 76$ cm, $V = 300$ cc).

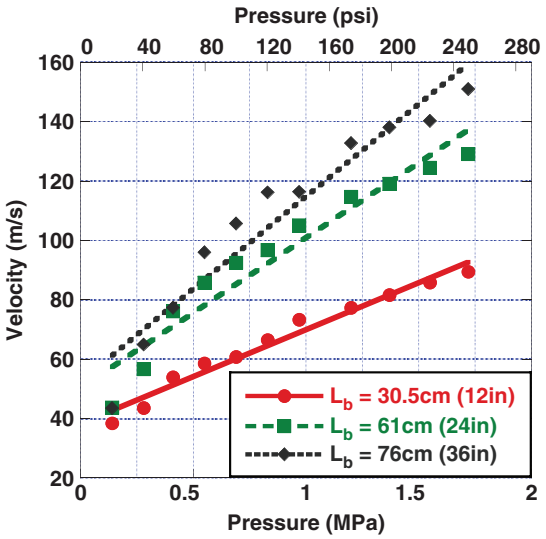

Figure 11 Effects of different barrel lengths on velocity with helium propellant ($M = 4$ g, $V = 300$ cc).

(out of 14), for air and helium respectively. The data for air tests was best fitted by a triangular probability density distribution, while the data for helium tests was best represented by a decaying exponential probability density distribution (Fig. 13).

Conclusions

A gas gun was designed to propel small projectiles into soil at a maximum velocity of 200 m/s. The gun was designed to operate using either compressed helium or air, and to be reconfigured for various barrel lengths and chamber volumes. A total of 515 tests spanning 85 test conditions were performed to determine the gun performance characteristics. The measured velocity was highly repeatable with an acceptable relative standard deviation averaging 3.8% for both air and helium. The isentropic expansion predicted the relative effects with different barrel lengths, projectile masses, and chamber volumes. An average efficiency of 57 and 70% was observed for air and helium propellants, when compared to the theoretical velocity expected from ideal gas expansion; the cause of which is attributed to possible choked flow in the trigger valve, gas blow-by around the projectile, and propagation effects due to sound speed limitations of the two gases.

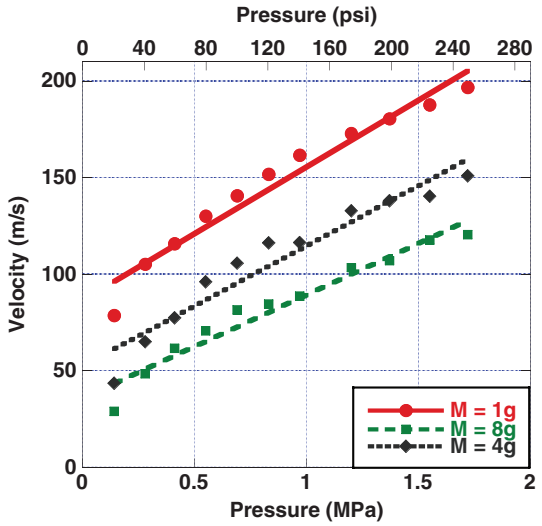

Figure 12 Effects of projectile mass on velocity with helium propellant ($L_b = 76$ cm, $V = 300$ cc).

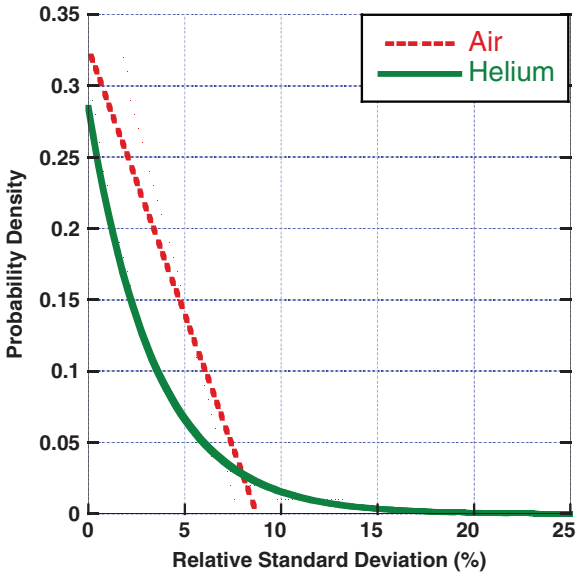

Figure 13 Probability distribution of relative standard deviations of velocities for air and helium tests.

Acknowledgments

The authors gratefully acknowledge the support of the Defense Threat Reduction Agency (DTRA) of the United States of America, Grant No: HDTRA1-10-1-0049. The first two authors were supported by the AMPS-CBSI Fellowship which is funded through NSF GK-12 Fellows Program Grant DGE-0741714 and the CBSI Initiative, which is funded by the Black Male Donor Collaborative, Brooklyn Community Foundation, J.P. Morgan Chase Foundation, Motorola Innovation Generation Grant, NY Space Grant Consortium, Xerox Foundation, and White Cedar Fund. Beneficial communications with Prof. John Borg and his students are gratefully acknowledged.

References

1. Zukas, J., Theodore, N., Swift, H., Greszczuk, L., and Curran, D., *Impact Dynamics*, Wiley Publishing, New York (1982).
2. Heuze, F.E., ''An Overview of Projectile Penetration into Geological Materials, with Emphasis on Rocks,'' *International Journal of Rock mechanics and Mining Science and Geomechanical Abstracts* **27**(1):1–14 (1990).
3. Omidvar, M., Iskander, M., and Bless, S., ''Response of Granular Media to Rapid Penetration,'' *International Journal of Impact Engineering* **66**:60–82 (2014). DOI: 10.1016/j.ijimpeng.2013.12.004
4. Guzman, I., and Iskander, M., ''Geotechnical Properties of Sucrose-Saturated Fused Quartz for Use in Physical Modeling,'' *Geotechnical Testing Journal* **36**(3):139–150 (2013). DOI: 10.1520/GTJ20130037
5. Guzman, I., Iskander, M., Suescun, E., and Omidvar, M., ''A Transparent Aqueous-Saturated Sand-Surrogate for use in Physical Modeling,'' *Acta Geotechnica* **9**(2):187–206 (2014). DOI: 10.1007/s11440-013-0247-2
6. Iskander, M., *Modeling with Transparent Soils, Springer-Verlag*, Berlin, Germany (2010).
7. Sadek, S., Iskander, M., and Liu, J., ''Accuracy of Digital Image Correlation for Measuring Deformations in Transparent Media,'' *ASCE Journal of Computing in Civil Engineering* **17**(2):88–96 (2003).
8. Liu, J., and Iskander, M., ''Adaptive Cross Correlation for Imaging Displacements in Soils,'' *ASCE Journal of Computing in Civil Engineering* **18**(1):46–57 (2004).
9. Iskander, M., and Liu, J., ''Spatial deformation measurement using transparent soil,'' *Geotechnical Testing Journal* **33**(4):1–7 (2010).
10. Liu, J., and Iskander, M., ''Laboratory Investigation of the Modeling Capacity of Synthetic Transparent Soils'' *Canadian Geotechnical Journal* **47**(4):451–460 (2010). DOI: 10.1139/T09-116
11. Thompson, J., 1975, ''Low-Velocity Impact Penetration of Low-Cohesion Soil Deposits,'' Ph.D. Dissertation, University of California, Berkeley, CA.
12. Borg, J.P., and Vogler, T.J., ''An experimental Investigation of a High Velocity Projectile Penetrating Sand,'' *Proceedings of the XIth International Congress and Exposition, Society for Experimental Mechanics Inc.*, Orlando, FL (2008).

13. Bresie, D., and Ingram, S., ''Coilgun Technology at the Center For Electromechanics, The University of Texas at Austin,'' *IEEE Transactions on Magnetics* **29**(1):648–654 (1993).
14. Hoff, A., *Airguns and Other Pneumatic Arms*, Barrie and Jenkins, London, UK (1972).
15. Borg, J., Morrisseya, M., Pericha, C., Voglerb, T., and Chhabildas, L., ''In Situ Velocity and Stress Characterization of a Projectile Penetrating a Sand Target: Experimental Measurements and Continuum Simulations,'' *International Journal of Impact Engineering* **51**:23–35 (2013).
16. White, F., *Fluid Mechanics*, 4th Edition, McGraw Hill, New York (1999).
17. Canning, T. N., James, C.S., and Seiff, A., 1970, ''Ballistic Range Techlonogy,'' *AGARD-AG-138*, NATO Science and Technology Organization.
18. Charters, A., ''Development of the High-Velocity Gas-Dynamics Gun,'' *International Journal of Impact Engineering* **5**(1–4):181–203 (1987).
19. Charters, A., ''The early years of aerodynamics ranges, light-gas guns, and high-velocity impact,'' *International Journal of Impact Engineering* **17**(1–3):151–182 (1995).
20. Considine, D., *Process Instruments and Controls Handbook*, 2nd Edition, McGraw-Hill Book Company, New York (1957).
21. Zappe, R.W., *Valve Selection Handbook*, 2nd Edition, Gulf Publishing Company, Houston, TX (1987).
22. Palisade Corporation. @Risk Software User Guide, Risk Analysis and Simulation Add-In for Microsoft Excel, Version 6, Palisade Corporation, 2013, URL http://www.palisade.com [accessed on 22 April 2013].